Microchimica Acta
https://doi.org/10.1007/s00604-019-3510-x

ORIGINAL PAPER

An impedimetric aptasensor for ultrasensitive detection of *Penicillin G* based on the use of reduced graphene oxide and gold nanoparticles

Ayat Mohammad-Razdari[1] · Mahdi Ghasemi-Varnamkhasti[1,2] · Zahra Izadi[1,2] · Ali A. Ensafi[3] · Sajad Rostami[1] · Maryam Siadat[4]

Received: 1 March 2019 / Accepted: 14 May 2019

Abstract

The authors describe an impedimetric aptasensor for *Penicillin G* (PEN) which is an important antibiotic. The method is based on the use of a pencil graphite electrode (PGE) modified with reduced graphene oxide (RGO) and gold nanoparticles (GNPs) for ultrasensitive detection of PEN. The morphology of a bare PGE, RGO/PGE, and GNP/RGO/PGE, and the functional groups on graphene oxide (GO) and RGO were studied using scanning electron microscopy and Fourier transform infrared spectroscopy. Electrochemical impedance spectroscopy was used for detection of PEN by measuring the charge transfer resistance (R_{ct}). Also, cyclic voltammetry was recorded at potential range of 0.30 to +0.70 V for PGE treatment. This aptamer-based assay has a wide linear range that extends from 1.0 fM to 10 μM, and a limit of detection as low as 0.8 fM. The method was applied to the determination of PEN in spiked milk from cow, sheep, goat and water buffalo. Recoveries ranged from 92% to 104%. The assay is fast, ultrasensitive, high reproducible, and selective over antibiotics such as streptomycin, tetracycline, and sulfadiazine.

Keywords Milk samples · Electrochemical impedance spectroscopy · Cyclic voltammetry · Antibiotic · DNA-modified pencil graphite electrode · Nanocomposite · Aptamer-based biosensor · Charge transfer resistance · Electrochemical aptasensor · Nanomaterials

Introduction

The excessive use of *Penicillin G* (PEN) leads to its residues in dairy products and poses risk to consumer health [1]. Therefore, rapid detection of antibiotics residues in milk and other food products is necessary to protect human health and maintain food security.

To date, different methods have been introduced for antibiotics detection, including polymerase chain reaction (PCR) [2], high performance liquid chromatography (HPLC) [3], chromatography-mass spectrometry/mass spectrometry (HPLC-MS/MS) [4], colorimetric [5], fluorescence [6], and surface resonance (SPR) [7]. Although the above mentioned methods are accurate and reliable for antibiotic detection, they require a complicated process, large and costly instrument, and professional user. Due to its simple operation, fast response, portability, being time-saving, and having miniaturized and cheap equipment, electrochemical aptasensor has attracted extensive attention for antibiotic detection [8–10].

Aptamers are short single-stranded oligonucleotides (DNA or RNA)with many unique benefits like e.g., accessibility, incomparable anti-fouling ability, individual three-dimensional (3D) structure, high stability, excellent affinity, recyclable synthesis, and inherent specificity [11, 12]. According to the mentioned features, aptamers are ideal for

Electronic supplementary material The online version of this article (https://doi.org/10.1007/s00604-019-3510-x) contains supplementary material, which is available to authorized users.

✉ Mahdi Ghasemi-Varnamkhasti
ghasemymahdi@gmail.com

Ayat Mohammad-Razdari
am.razdari@gmail.com

[1] Department of Mechanical Engineering of Biosystems, Shahrekord University, Shahrekord 8818634141, Iran

[2] Nanotechnology Research Center, Shahrekord University, Shahrekord 8818634141, Iran

[3] Department of Chemistry, Isfahan University of Technology, Isfahan 84156, Iran

[4] LCOMS, Université de Lorraine, EA 7306, F-57000 Metz, France

Published online: 23 May 2019

electrochemical biosensors application. In order to increase the sensitivity of aptasensors, a variety of nanomaterials can be utilized.

Graphene is formed by carbon sheets. Due to their unique structure, electrical conductivity, chemical stability, and thermal activities, graphene and its derivatives have attracted much attention as novel nanomaterials [13]. Owing to its thermal properties and electrochemical efficiency, reduced grapheme oxide (RGO) is a very promising material in biosensor applications [14]. Todays, the preparation of different nanocomposites by combining RGO with various materials such as metal oxides, polymers, and gold nanoparticles (GNPs) has been the subject of considerable interest [15].

On the other hand, as an upmost alternative among noble metals, GNPs are promising nanomaterials in the field of aptasensing due to their electrochemical activity, being ecofriendly, and having excellent chemical inertness and good catalyst attributes [16]. The combination of RGO and GNP as a nanocomposite provides higher electrochemical activity and high electron transfer capability [17]. Nowadays, GNP/RGO nanocomposite has been widely used in electrochemical biosensors [18, 19].

In the current research, an ultrasensitive and selective electrochemical aptasensor based on GNP/RGO nanocomposite modified pencil graphite electrode (PGE) for PEN detection was developed. The important parameters investigated include: dynamic range and limit of detection (LOD) of the electrochemical aptasensor for impedimetric detection of PEN in milk samples,. To this purpose, the charge transfer resistance (Rct) between Aptamer/GNP/RGO and PEN was measured using electrochemical impedance spectroscopy (EIS) method. The method was effectively used for detection of PEN in milk samples; additionally, the aptasensor had good stability, repeatability and selectivity with low LOD and a broad dynamic range. To the best of our knowledge, the aptasensor has not been yet used as bio-recognition based on PGE modified with GNP/RGO nanocomposite for PEN detection.

Experimental

Chemicals and reagents

Oligonucleotides with the following sequences were purchased from Microsynth AG (www.microsynth.ch, Balgach, Switzerland): A 19-mer thiolated PEN-binding aptamer with a sequence of 5'-SH-TTA GTT GGG GTT CAG TTG G-3′ (all oligonucleotides with HPLC purification and optical density of 8.78). The aptamer was diluted with deionized (DI) water and stored as a stock solution (100 μM) at −20 °C for the next experiments. All solutions were prepared with DI water. Hydrochloric acid (HCl), gold chloride ($HAuCl_4.3H_2O$), diethyl ether, potassium permanganate ($KMnO_4$), hydrogen peroxide (H_2O_2), potassium ferricyanide ($K_3[Fe(CN)_6]$), and potassium ferrocyanide ($K_4[Fe(CN)_6]$) were obtained from Sigma-Aldrich Inc. (www.sigmaaldrich.com, USA). Further, graphite powder, potassium chloride (KCl), sodium borohydride ($NaBH_4$), sulfuric acid (H_2SO_4), sodium nitrate ($NaNO_3$), potassium nitrate (KNO_3), dimethylformamide (DMF), dithiothreitol (DTT), and ethyl acetate were acquired from Merck Chemicals (www.merckmillipore.com). Phosphate buffer solution (0.1 M, pH of 7.0) was prepared with a stock standard solution of NaH_2PO_4 and Na_2HPO_4.

Instrumentation and characterization

Electrochemical experiments were run using Ivium potentiostat/galvanostat (Vertex1, the Netherlands) coupled with Ivium software connected to a laptop. A common three-electrode system, including a bare or modified PGE as a working electrode, a platinum wire as an auxiliary electrode (with a length of 3 mm) and an Ag/AgCl as a reference electrode (with KCL of 3 M as reference electrolyte), were applied in voltammetry and impedimetric measurements. All electrochemical measurements, including cyclic voltammetry (CV) and EIS, were carried out in a solution containing 5.0 mM of $Fe(CN)_6^{4-/3-}$ in 0.1 M KCl as a redox probe. Potential, amplitude, and frequency range of EIS were 150 mV, 10 mV, and 0.01 to 10^5 Hz, respectively. CV was run at the potential range of −0.3 to 0.70 V with a scan rate of 50 mV s^{-1}. All experiments were done at room temperature (23 ± 1 °C).

Fourier transform infrared spectroscopy (FTIR) was acquired on JASCO 630 (Japan) to obtain the presence/absence of functional groups on GO and RGO. The FTIR spectrum was employed in a range of 4000–500 cm^{-1}. Images of morphological changes were recorded using ZEISS EVO (Germany) scanning electron microscope (SEM) for characterization of bare PGE, RGO/PGE, and GNP/RGO/PGE.

Synthesis of graphene oxide (GO)

GO was prepared by a modified Hummer's method [20]. First, GO was synthesized from graphite powder. In brief, 2.0 g of graphite powder (particle size of 70 μm) was combined in a mixed solution of H_2SO_4 (96 mL) and $NaNO_3$ (2.0 g). Then regularly, 12.5 g of $KMnO_4$ as an oxidizing agent was added to the mixture for 1 h (10 times with a time interval of 5 min). The mixture was continuously stirred for 1 h in oil bath conditions (35 °C) and 200 mL of distilled water was added to it (in an ice bath conditions). Then the solution was stirred for 15 min in the oil bath (98 °C) and 600 mL of distilled water was added to it. After this step, 16 mL of H_2O_2 (30%) and 10 mL of HCl (10% *v/v*) were combined in the mixture

solution at room temperature. The composition produced until this stage was GO, which should be rinsed to reach a neutral pH. For purification of GO, the solvent and anti-solvent extraction methods were used and GO was dispersed in methanol. Then, by adding the diethyl ether, it was dissolved and purified. In the end, the GO solution was dried at room temperature for 48 h.

Preparation of reduced graphene oxide (RGO)

In order to prepare RGO, 100 mL of GO suspension (2.5 mg mL^{-1}) was prepared in distilled water. Then, the suspension was put in an ice bath. After that, 12.5 g of $NaBH_4$ was prepared in 50 mL of cold water and was mixed with GO suspension (in an ice bath) drop by drop. Then it was regularly stirred for 12 h at room temperature. Finally, the RGO was separated by filtration and rinsed with distilled water several times. The black solution obtained in the previous step was dried at room temperature. For all of the experiments, 0.005 g of RGO was dispersed in 5 mL of DMF and the mixture was stirred under sonication for 30 min to acquire a well-dispersed suspension.

Fabrication of the aptasensor

First of all, bare PGE was modified using CV technique. To this purpose, the PGE was treated in sodium hydroxide solution (1.0 M) with a constant potential of +1.50 V, a scan rate of 40 mV s^{-1} with number cycle of 10 for 12 min. In order to immobilize the RGO on the surface of the working electrode, the PGE modified was dipped into RGO solution for 90 min. The electrode was then immersed into a phosphate buffer solution and CV was recorded at −0.30 to +0.70 V (10 cycles). Immobilization of GNP on RGO/PGE surface was performed using CV in a potential range of −0.50 to +1.50 V, a scan rate of 5 mV s^{-1} into a 3.0 mM of $HAuCl_4.3H_2O$ solution. Finally, GNP/RGO/PGE was dipped in a 0.1 M KNO_3, and CV was performed in a potential range of −0.50 to +1.50 V (10 cycles).

To immobilize the aptamer at the surface of GNP/RGO/PGE, the working electrode was laid in aptamer solution (25.0 μM) for 80 min at room temperature. Then the electrode was slowly rinsed with DI water to remove any unbounded aptamer on the Aptamer/GNP/RGO/PGE surface and was dried at room temperature. The graphical image of GNP/RGO/PGE aptasensor for detection of PEN is shown in Scheme 1.

Detection of penicillin G

In the current study, the aptasensor was used to detect PEN in milk samples. Additionally, *streptomycin, tetracycline,* and *sulfadiazine* were applied to examine the aptasensor selectivity. The aptasensor was immersed into a 0.9% NaCl solution (as a blank solution). In order to detect PEN, the aptasensor was placed in the PEN solution for 60 min (optimized incubation time). After that, PEN/Aptamer/GNP/RGO/PGE was slowly rinsed with DI water to eliminate the unbounded PEN. Then EIS was run in a solution containing 5 mM of $Fe(CN)_6^{4-/3-}$ in 0.1 M KCl. The Rct of the fabricated aptasensor was recorded before and after PEN bounding to make sure of the aptasensor efficiency. Different concentration of PEN from 1×10^{-16} to 1×10^{-6} M were prepared to check the aptasensor performance. EIS was used to draw calibration plot using ΔRct vs the logarithm of different concentrations of PEN.

Preparation of the milk samples

Raw milk was acquired from the livestock farm and stored at 4 °C. Milk samples, including cow, sheep, goat and water buffalo's milk were considered as the real samples. Before testing the sample, the milk was firstly diluted with a buffer solution in a ratio of 1:10 (*v/v*). Milk is a complex matrix, as it contains fat, carbohydrates, and protein, to remove the protein and fat, it was centrifuged at 30000 rpm for 60 min. To spike different concentrations of PEN and compute recovery percentage, the middle layer related to pure milk was stored. This process was replicated for all of the actual samples.

Results and discussion

Structural analysis

FTIR spectra and SEM characterizations were used to verify the successful immobilization of nanomaterials of the PGE surface (Fig. 1a and b). As shown in Fig. 1a, the functionalized groups of GO and RGO are more confirmed using FTIR data. In FTIR spectra of the GO, the broad peak at 3420 cm^{-1} was related to stretching bands of O–H groups and intercalated water molecules [21]. The peaks at 1571 cm^{-1} and 1724 cm^{-1} correspond to the skeletal vibrations of oxidized graphitic domains and -C=O (carboxylic acid) stretching vibrations on GO sheets, respectively [22]. The two absorption peaks at 1165 cm^{-1} and 1035 cm^{-1} can be assigned to the C–O stretching vibrations and C-O-C stretching, respectively [23]. The reduction of GO was also investigated using FT-IR data. As it can be seen in Fig. 1a, all the intensities of the peaks corresponding to the oxygen-containing functionalities of RGO were decreased compared to those of GO and even some were disappeared. This showed that most of the oxygen-containing groups were released from GO by reduction processing [24].

The results of SEM characterization are presented for the bare PGE (a), RGO/PGE (b), and GNP/RGO/PGE (c) in Fig.

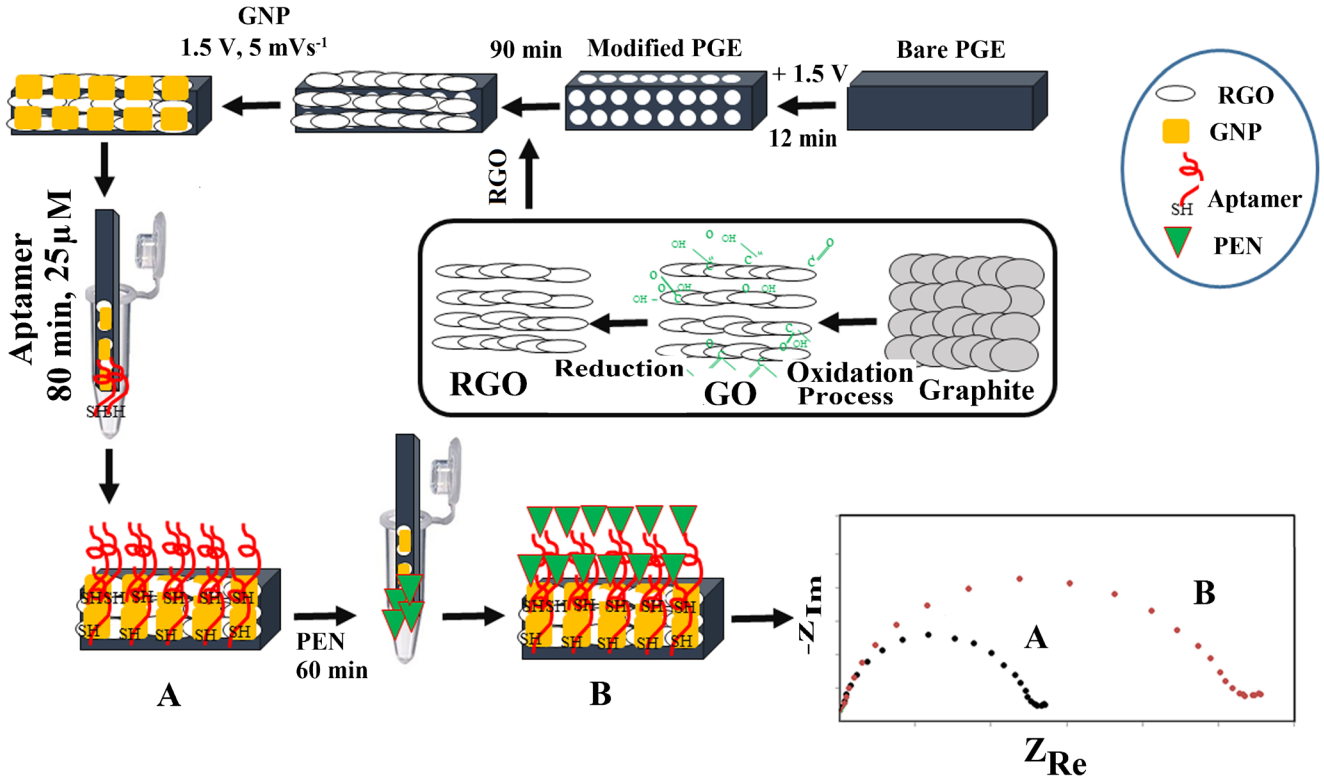

Scheme 1 Fabrication of the aptasensor for PEN detection

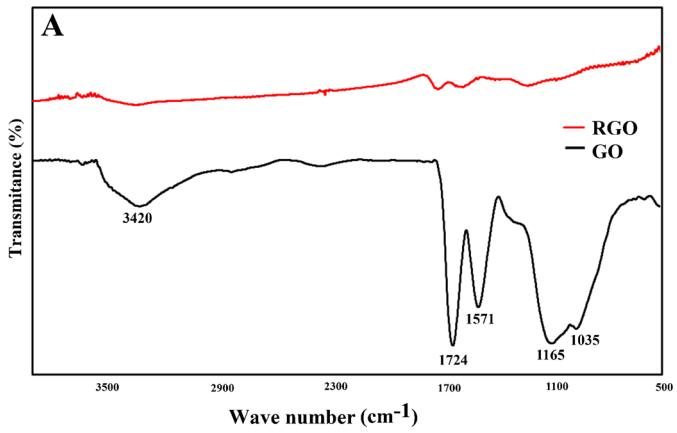

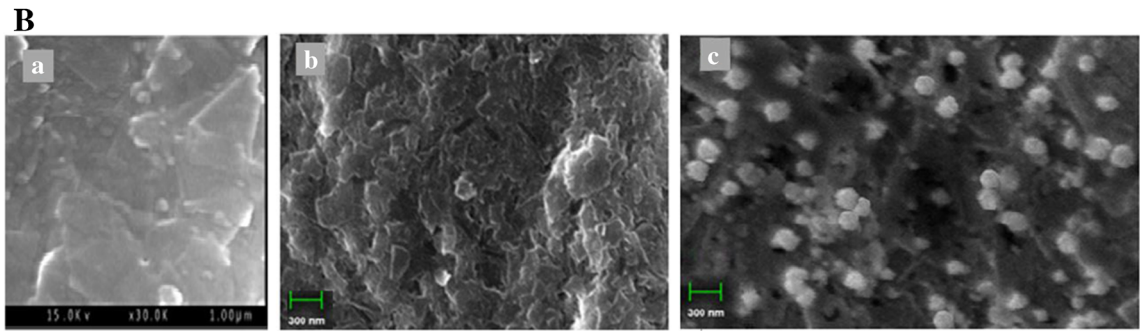

Fig. 1 **a** FT-IR spectra of GO (black line) and RGO (red line); **b** SEM images of (a): bare PGE, (b): RGO/PGE, and (c): GNP/RGO/PGE

1b. Figure 1b(a) illustrates uniform smooth surface related to the bare PGE. Figure 1b(b) depicts the RGO layers aggregated due to the $\pi - \pi$ stacking within the wrinkled paper-like structure of RGO sheets. Figure 1b(c) displays GNPs morphology when it is assembled on the surface of RGO/PGE. All the above characterizations show that GNP and RGO have been successfully placed on the surface of the PGE.

Electrochemical measurement of PEN

To check the electrochemical behaviour of PGE modified with different materials, CV and EIS results of the bare and modified PGE were evaluated. Electrochemical measurement results are presented in Fig. 2a and b. Immobilization of RGO and GNP on PGE treated surface increased the kinetic of the electron transfer, additionally, the peak current of the redox probe $Fe(CN)_6^{4-/3-}$ was significantly amplified by RGO and GNP compared to the bare PGE. It happened because of the excellent conductivity of RGO and GNP and their high electroactive surface area on the electrode. In order to immobilize the aptamer on the surface of GNP/RGO/PGE, the thiolated aptamer was self-assembled at the surface of GNP/RGO/PGE. According to Fig. 2a, the peaks current of aptamer and PEN are decreased in comparison to the bare PGE. This result can be described by the electrostatic repulsion between negative charge of redox probe $Fe(CN)_6^{4-/3-}$ and the electrode [25].

Except for the CV curves, EIS curves of the modified electrodes were also recorded to check the charge transfer of the PGE surface modification. EIS is an appropriate

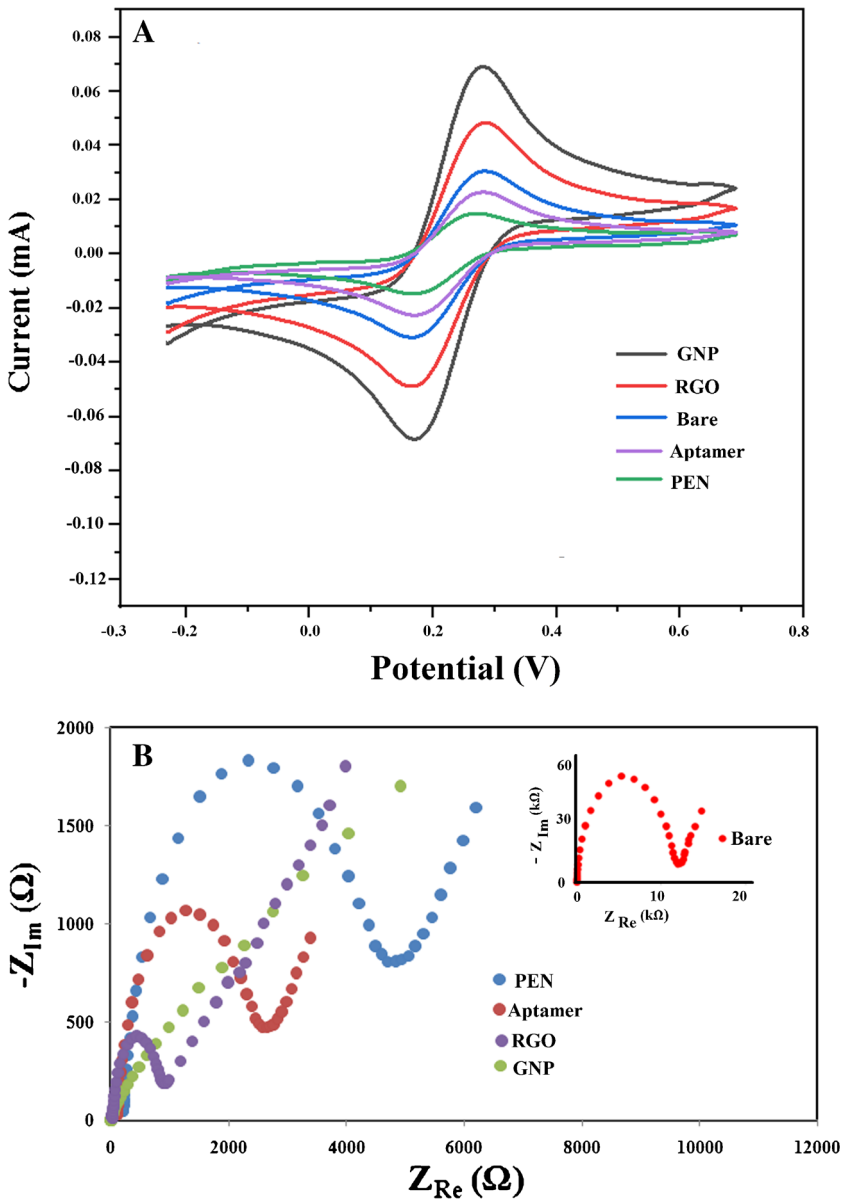

Fig. 2 **a** CV and **b** EIS curves of the bare and modified PGE in a solution containing 5.0 mM of $Fe(CN)_6^{4-/3-}$ in the presence of 0.1 M KCl

technique for demonstration of changes on the modified electrodes surface. In Nyquist curve of EIS, the semicircle part at the higher frequencies range corresponds to an electron transfer-limited process and the linear portion at the lower frequencies is related to a diffusion process [26]. The increased diameter of the semicircle indicates a raised Rct. According to Fig. 2b, after modification of PGE with RGO and GNP, the value of Rct is decreased compared to the bare PGE. It happened due to the high conducting capacity of RGO and GNP and the increased electron transfer through immobilization of aptamer on GNP/RGO/PGE surface, which leads to the formation of a resistant negatively charged layer at the electrode surface. Additionally, the Rct value of Aptamer/GNP/RGO/PGE was enhanced compared to RGO/PGE, and GNP/RGO/PGE. After the incubation of aptasensor with PEN, the Rct value dramatically increased. The reason can be because of PEN capturing on reaction sites of Aptamer/GNP/RGO/PGE to the (aptamer strands) [26]. As the peak current and Rct belong to a couple of reciprocal variables, the change trend of peak current was actualy opposite to that of the Rct value [27]. On the other hand, the CV results were in agreement with those of EIS.

Optimization of method

The following parameters were optimized: (a) immobilization time for RGO; (b) immobilization time for aptamer; (c) concentration of aptamer; (d) interaction time of PEN. Respective text and Figures on optimizations are given in the Electronic Supporting Material (Fig. S1A-D). In short, the following experimental conditions were found to give the best results: (a) Best immobilization time for RGO: 90 min; (b) Best immobilization time for aptamer: 80 min; (c) Best concentration of aptamer: 25 μM; (d) interaction time of PEN: 60 min.

Detection performance of the aptasensor

EIS method was run to prepare calibration plot, by plotting the ΔR_{ct} (the interaction between PEN and the aptasensor) vs. the logarithmic concentrations of PEN. In the current work, ΔRct values are correlated with concentrations of PEN. The calibration plot of the designed aptasensor demonstrated a linear dynamic range from 1 fM to 10 μM with a regression equation of $\Delta R_{ct} = 119.3 \mathrm{Log} C_{PEN} + 2602$ ($R^2 = 0.98$) (Fig. 3a). LOD for PEN detection (based on $3S_b/m$, where S_b is the standard deviation of blank samples and m is the slope of the

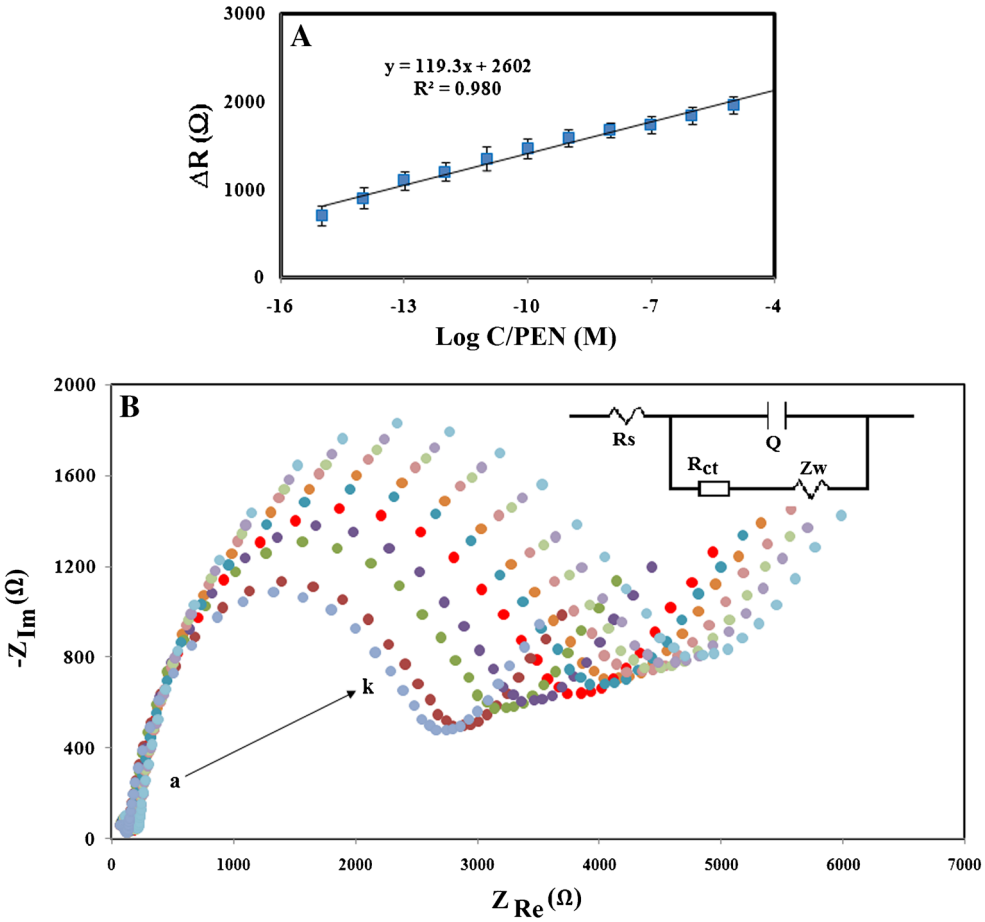

Fig. 3 **a** Calibration plot for ΔR_{ct} vs. Log concentration of PEN; **b** Nyquist plot for different concentration of PEN, (a-k) 1.0×10^{-15}, 1.0×10^{-14}, 1.0×10^{-13}, 1.0×10^{-12}, 1.0×10^{-11}, 1.0×10^{-10}, 1.0×10^{-9}, 1.0×10^{-8}, 1.0×10^{-7}, 1.0×10^{-6}, 1.0×10^{-5} M, respectively; In 5.0 mM $Fe(CN)_6^{4-/3-}$ (0.1 M KCl solution); The error bars illustrated the standard deviation (SD) ($n = 3$). Insert the employed Randles circuit for fitting the EIS results was demonstrated

Table 1 A brief comparison between the aptasensor and other reported methods

Sensing system	Signal mode	Linear range	LOD	Reference
Electrochemical aptasensor	Impedimetric	10^2–10^4 μg mL^{-1}	10 μg mL^{-1}	[28]
Piezoelectric immunosensors	Voltammetry	2.5–25 ng mL^{-1}	0.8 ng mL^{-1}	[29]
Fluorescent aptasensor	Fluorescence intensity	0.1–100 ng mL^{-1}	0.07 ng mL^{-1}	[30]
Electrochemical aptasensor	Voltammetry	1×10^{-4}-5×10^{-4} M	1×10^{-6} M	[31]
Surface-enhanced Raman scattering	Amperometric	1×10^{-8}-1×10^{-3} M	2.54×10^{-9} M	[32]
Fluorescence detection	Polarization emission spectra	–	1×10^{-9} M	[33]
Electrochemical aptasensor	Amperometric	1×10^{-10}-1×10^{-7} M	32×10^{-12} M	[8]
Electrochemical aptasensor	Impedimetric	1×10^{-10}-1×10^{-6} M	–	[34]
Electrochemical aptasensor	Amperometric	2×10^{-11}-4×10^{-8} M	4×10^{-12} M	[35]
Electrochemical aptasensor	Voltammetry	5×10^{-14}–5×10^{-8} M	15×10^{-15} M	[9]
Electrochemical aptasensor	Impedimetric	1×10^{-5}-1×10^{-15} M	8×10^{-16} M	This method

calibration plot in the linear range) was computed to be 0.8 fM, which is less than the maximum concentration of residue (9.93 nM) based on the European Union regulations [8].

The EIS results (Fig. 3b) show that the semicircular diameters in the Nyquist plots, which are proportional to the Rct of the working electrode, increased by increasing PEN concentration. The relationship between Rct and PEN concentration was also checked. The Randles equivalent circuit was employed for fitting EIS data, where Rs is the electrolyte resistance. The impedance of the faradaic reaction includes Rct, the Warburg impedance (Z_w), and the double layer capacitance (Q) in a parallel circuit (inset of Fig. 3b). The detection performances are compared to some of the reported methods and the results are listed in Table 1. According to Table 1,

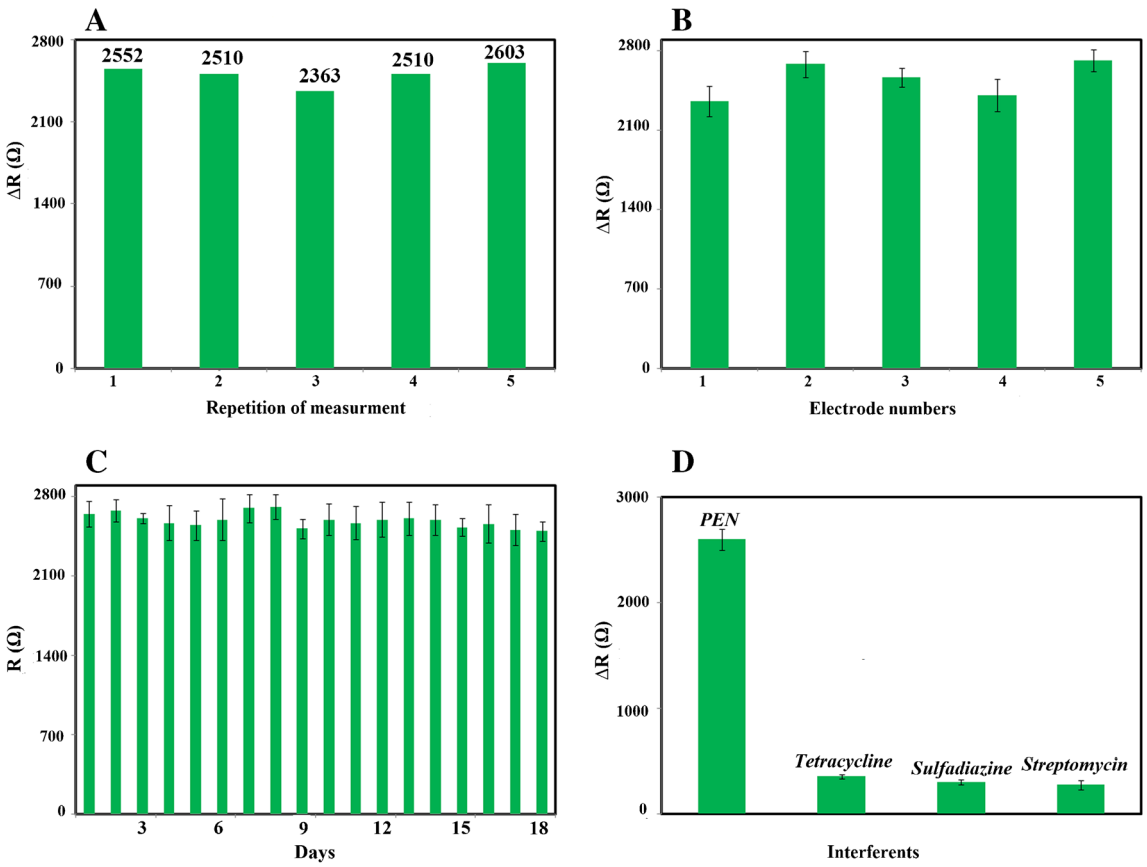

Fig. 4 **a** Repeatability of the aptasensor with five measurements; **b** Reproducibility of the aptasensor with five independent electrodes, **c** storage stability for 18 days, and **d** selectivity of the aptasensor towards PEN in the presence of other antibiotics. The error bars represented the standard deviation (SD) ($n = 3$)

Table 2 Detection of PEN in milk samples using fabricated aptasensor

Type of milk	Added (M)	Found [a] (M)	Recovery (%)	RSD (%)
Cow milk	1×10^{-9}	$(0.96 \pm 0.06) \times 10^{-9}$	96.2	6.25
	1×10^{-11}	$(0.92 \pm 0.07) \times 10^{-11}$	92.3	7.61
Sheep milk	1×10^{-9}	$(0.95 \pm 0.06) \times 10^{-9}$	95.3	6.31
	1×10^{-11}	$(1.04 \pm 0.08) \times 10^{-11}$	104.0	7.69
Goat milk	1×10^{-9}	$(0.95 \pm 0.07) \times 10^{-9}$	94.7	7.36
	1×10^{-11}	$(0.93 \pm 0.09) \times 10^{-11}$	93.4	9.67
Water buffalo milk	1×10^{-9}	$(0.96 \pm 0.0.07) \times 10^{-9}$	96.0	7.29
	1×10^{-11}	$(1.03 \pm 0.0.09) \times 10^{-11}$	103.0	8.73

[a] Average of three measurements ± SD

LOD and the linear dynamic range acquired for the aptasensor are better than those reported in previous methods.

Repeatability, reproducibility, stability, and selectivity of the aptasensor

To study the repeatability of the PEN/Aptamer/GNP/RGO/PGE, one electrode was fabricated and immersed into a PEN solution, and then, ΔR_{ct} value was recorded for five successive measurements using EIS method (Fig. 4a). According to the results, the relative standard deviation (RSD) of 3.5% was obtained, indicating that the aptasensor exhibits a satisfactory repeatability.

Reproducibility of the impedimetric aptasensor was measured using five modified electrodes prepared independently under the same conditions for the EIS measurements of the analyte. As shown in Fig. 4b, ΔRct results almost are acceptable values (RSD = 6.25%, n = 5). Furthermore, the long-term stability was investigated by storing five electrodes at 4 °C, which were continuously measured every day for 18 days. As illustrated in Fig. 4c, it was found that about 94% of the initial value was retained after 18 days, indicating the good stability of the aptasensor.

To evaluate the selectivity of the PEN aptasensor based on GNP/RGO/PGE, three other antibiotics were considered as possible interferences, including *streptomycin, tetracycline* and *sulfadiazine* (with the same concentration and under optimal conditions). According to Fig. 4d, all interferences show negligible signal compared to PEN, indicating that the aptasensor can effectively discriminate between PEN and other interferences.

Analysis of aptasensor performance in real samples

In order to evaluate the practical application of the aptasensor in real samples, the biosensor was employed to determine PEN residues in four types of milk including cow, sheep, goat, and water buffalo's milk samples. As can be seen in Table 2, the recovery for the milk sample varies from 92% to 104% and the RSD varies from 6% to 9%. Therefore, this method shows great potential for practical use in the detection of PEN residues in other food samples.

Conclusions

A novel ultrasensitive aptesensor based on RGO and GNPs modified PGE for determining antibiotic residue in milk samples was developed. In the optimum conditions, the aptasensor detected PEN in a concentration range from 1 fM to 10 μM with LOD of 0.8 fM. The aptasensor for PEN detection denoted a high selectivity, good reproducibility and acceptable stability. The suitable results of our work indicate that the aptasensor is a promising, low-cost, and highly sensitive and selective approach for PEN determination and may have potential application in early screening of food samples.

Acknowledgements This work has been supported by the Center for International Scientific Studies & Collaboration (CISSC) and French Embassy in Iran.

Compliance with ethical standards The author(s) declare that they have no competing interests.

References

1. Prado TM, Foguel MV, Gonçalves LM, Sotomayor M, Del PT (2015) β-Lactamase-based biosensor for the electrochemical determination of benzylpenicillin in milk. Sensors Actuators B Chem 210:254–258. https://doi.org/10.1016/j.snb.2014.12.108
2. Ali R, Al-Achkar K, Al-Mariri A, Safi M (2014) Role of polymerase chain reaction (PCR) in the detection of antibiotic-resistant Staphylococcus aureus. Egypt J Med Hum Genet 15:293–298. https://doi.org/10.1016/j.ejmhg.2014.05.003
3. Moudgil P, Bedi JS, Aulakh RS, Gill JPS, Kumar A (2019) Validation of HPLC multi-residue method for determination of

fluoroquinolones, tetracycline, Sulphonamides and chloramphenicol residues in bovine Milk. Food Anal Methods 12:338–346. https://doi.org/10.1007/s12161-018-1365-0
4. Bogialli S, Capitolino V, Curini R, Di Corcia A, Nazzari M, Sergi M (2004) Simple and rapid liquid chromatography−tandem mass spectrometry confirmatory assay for determining amoxicillin and ampicillin in bovine tissues and Milk. J Agric Food Chem 52:3286–3291. https://doi.org/10.1021/jf0499572
5. Koch C, Poghossian A, Schöning MJ, Wege C (2018) Penicillin detection by tobacco mosaic virus-assisted colorimetric biosensors. Nanotheranostics 2:184–196. https://doi.org/10.7150/ntno.22114
6. Yang Q, Zhou L, Wu YX, Zhang K, Cao Y, Zhou Y, Gan N (2018) A two dimensional metal–organic framework nanosheets-based fluorescence resonance energy transfer aptasensor with circular strand-replacement DNA polymerization target-triggered amplification strategy for homogenous detection of antibiotics. Anal Chim Acta 1020:1–8. https://doi.org/10.1016/j.aca.2018.02.058
7. Luo Q, Yu N, Shi C, Wang X, Wu J (2016) Surface plasmon resonance sensor for antibiotics detection based on photo-initiated polymerization molecularly imprinted array. Talanta 161:797–803. https://doi.org/10.1016/j.talanta.2016.09.049
8. Wang T, Yin H, Zhang Y, Wang L, Du Y, Zhuge Y, Ai S (2019) Electrochemical aptasensor for ampicillin detection based on the protective effect of aptamer-antibiotic conjugate towards DpnII and Exo III digestion. Talanta 197:42–48. https://doi.org/10.1016/j.talanta.2019.01.010
9. Shen Z, Cao Y, Hong F, Zhang K, Hu F, Wu D, Gan N (2019) Multiplexed electrochemical aptasensor for antibiotics detection using metallic-encoded apoferritin probes and double stirring bars-assisted target recycling for signal amplification. Talanta 197:491–499. https://doi.org/10.1016/j.talanta.2018.12.018
10. Yang L, Ni H, Li C, Zhang X, Wen K, Ke Y, Wang Z (2019) Development of a highly specific chemiluminescence aptasensor for sulfamethazine detection in milk based on in vitro selected aptamers. Sensors Actuators B Chem 281:801–811. https://doi.org/10.1016/j.snb.2018.10.143
11. Li F, Yu Z, Han X, Shi W, Liu Y, Yan H, Zhang G (2018) A signal-on electrochemical aptasensor for highly sensitive and specific detection of kanamycin based on target-induced signaling probe shifting mechanism. Sensors Actuators B Chem 273:480–487. https://doi.org/10.1016/j.snb.2018.06.076
12. Razavipanah I, RounaghiG H, Deiminiat B, Damirchi S, Abnous K, Izadyar M, Khavani M (2019) A new electrochemical aptasensor based on MWCNT-SiO2@au core-shell nanocomposite for ultrasensitive detection of bisphenol a. Microchem J 146:1054–1063. https://doi.org/10.1016/j.microc.2019.02.018
13. Jiang WS, Xin W, Xun S, Chen SN, Gao XG, Liu ZB, Tian JG (2017) Reduced graphene oxide-based optical sensor for detecting specific protein. Sensors Actuators B Chem 249:142–148. https://doi.org/10.1016/j.snb.2017.03.175
14. Wang Y, Sauriat-Dorizon H, Korri-Youssoufi H (2017) Direct electrochemical DNA biosensor based on reduced graphene oxide and metal loporphyrin nanocomposite. Sensors Actuators B Chem 251:40–48. https://doi.org/10.1016/j.snb.2017.04.128
15. Özcan A, Topçuoğulları D, Özcan AA (2019) Fenitrothion sensing with reduced graphene oxide decorated fumed silica nanocomposite modified glassy carbon electrode. Sensors Actuators B Chem 284:179–185. https://doi.org/10.1016/j.snb.2018.12.122
16. Chen DJ, Zhang QL, Feng JX, Ju KJ, Wang AJ, Wei J, Feng JJ (2015) One-pot wet-chemical co-reduction synthesis of bimetallic gold–platinum nanochains supported on reduced graphene oxide with enhanced electrocatalytic activity. J Power Sources 287:363–369. https://doi.org/10.1016/j.jpowsour.2015.04.080
17. Piovesan JV, Santana ER, Spinelli A (2018) Reduced graphene oxide/gold nanoparticles nanocomposite-modified glassy carbon electrode for determination of endocrine disruptor methylparaben. J Electroanal Chem 813:163–170. https://doi.org/10.1016/j.jelechem.2018.02.025
18. Li X, Liu L, Xu Z, Wang W, Shi J, Liu L, Jing M, Li F, Zhang X (2019) Gamma irradiation and microemulsion assisted synthesis of monodisperse flower-like platinum-gold nanoparticles/reduced graphene oxide nanocomposites for ultrasensitive detection of carcinoembryonic antigen. Sensors Actuators B Chem 287:267–277. https://doi.org/10.1016/j.snb.2019.02.026
19. Jian JM, Fu L, Ji J, Lin L, Guo X, Ren TL (2018) Electrochemically reduced graphene oxide/gold nanoparticles composite modified screen-printed carbon electrode for effective electrocatalytic analysis of nitrite in foods. Sensors Actuators B Chem 262:125–136. https://doi.org/10.1016/j.snb.2018.01.164
20. Rezaei B, Jamei HR, Ensafi AA (2018) An ultrasensitive and selective electrochemical aptasensor based on RGO-MWCNTs/chitosan/carbon quantum dot for the detection of lysozyme. Biosens Bioelectron 115:37–44. https://doi.org/10.1016/j.bios.2018.05.012
21. Kassaee MZ, Motamedi E, Majdi M (2011) Magnetic Fe3O4-graphene oxide/polystyrene: fabrication and characterization of a promising nanocomposite. Chem Eng J 172:540–549. https://doi.org/10.1016/j.cej.2011.05.093
22. Nia PM, Abouzari-Lotf E, Woi PM, Alias Y, Ting TM, Ahmad A, Jusoh NW (2019) Electrodeposited reduced graphene oxide as a highly efficient and low-cost electrocatalyst for vanadium redox flow batteries. Electrochim Acta 297:31–39. https://doi.org/10.1016/j.electacta.2018.11.109
23. Guo HL, Wang XF, Qian QY, Wang FB, Xia XH (2009) A green approach to the synthesis of graphenen anosheets. ACS Nano 3:2653–2659. https://doi.org/10.1021/nn900227d
24. Eksin E, Zor E, Erdem A, Bingol H (2017) Electrochemical monitoring of biointeraction by graphene-based material modified pencil graphite electrode. Biosens Bioelectron 92:207–214. https://doi.org/10.1016/j.bios.2017.02.016
25. Izadi Z, Sheikh-Zeinoddin M, Ensafi AA, Soleimanian-Zad S (2016) Fabrication of an electrochemical DNA-based biosensor for Bacillus cereus detection in milk and infant formula. Biosens Bioelectron 80:582–589. https://doi.org/10.1016/j.bios.2016.02.032
26. Ensafi AA, Akbarian F, Heydari-Soureshjani E, Rezaei B (2018) A novel aptasensor based on 3D-reduced graphene oxide modified gold nanoparticles for determination of arsenite. Biosens Bioelectron 122:25–31. https://doi.org/10.1016/j.bios.2018.09.034
27. Jin H, Zhao C, Gui R, Gao X, Wang Z (2018) Reduced graphene oxide/nile blue/gold nanoparticles complex-modified glassy carbon electrode used as a sensitive and label-free aptasensor for ratiometric electrochemical sensing of dopamine. Anal Chim Acta 1025:154–162. https://doi.org/10.1016/j.aca.2018.03.036
28. Rosati G, Ravarotto M, Scaramuzza M, De Toni A, Paccagnella A (2019) Silver nanoparticles inkjet-printed flexible biosensor for rapid label-free antibiotic detection in milk. Sensors Actuators B Chem 280:280–289. https://doi.org/10.1016/j.snb.2018.09.084
29. Karaseva NA, Ermolaeva TN (2014) Piezoelectric immunosensors for the detection of individual antibiotics and the total content of penicillin antibiotics in foodstuffs. Talanta 120:312–317. https://doi.org/10.1016/j.talanta.2013.12.018
30. Luo Z, Wang Y, Lu X, Chen J, Wei F, Huang Z, Duan Y (2017) Fluorescent aptasensor for antibiotic detection using magnetic bead composites coated with gold nanoparticles and a nicking enzyme. Anal Chim Acta 984:177–184. https://doi.org/10.1016/j.aca.2017.06.037
31. Yu ZG, Lai RY (2018) A reagentless and reusable electrochemical aptamer-based sensor for rapid detection of ampicillin in complex samples. Talanta 176:619–624. https://doi.org/10.1016/j.talanta.2017.08.057
32. Chen Y, Li X, Yang M, Yang L, Han X, Jiang X, Zhao B (2017) High sensitive detection of penicillin G residues in milk by surface-

enhanced Raman scattering. Talanta 167:236–241. https://doi.org/10.1016/j.talanta.2017.02.022

33. Pennacchio A, Varriale A, Scala A, Marzullo VM, Staiano M, D'Auria S (2016) A novel fluorescence polarization assay for determination of penicillin G in milk. Food Chem 190:381–385. https://doi.org/10.1016/j.foodchem.2015.05.127
34. Daprà J, Lauridsen LH, Nielsen AT, Rozlosnik N (2013) Comparative study on aptamers as recognition elements for antibiotics in a label-free all-polymer biosensor. Biosens Bioelectron 43: 315–320. https://doi.org/10.1016/j.bios.2012.12.058
35. Wang X, Dong S, Gai P, Duan R, Li F (2016) Highly sensitive homogeneous electrochemical aptasensor for antibiotic residues detection based on dual recycling amplification strategy. Biosens Bioelectron 82:49–54. https://doi.org/10.1016/j.bios.2016.03.055